Novel CD44-Targeting and pH/redox Dual-Stimuli Responsive Core-Shell Nanoparticles Loading Triptolide to Combat Breast Cancer Growth and Lung Metastasis

Jinfeng Shi
Chengdu University of Traditional Chinese Medicine
Yali Ren
Chengdu University of Traditional Chinese Medicine
Jiaqi Ma
Chengdu University of Traditional Chinese Medicine
Xi Luo
Chengdu University of Traditional Chinese Medicine
Jiaxin Li
Chengdu University of Traditional Chinese Medicine
Yihan Wu
Chengdu University of Traditional Chinese Medicine
Huan Gu
Chengdu University of Traditional Chinese Medicine
Chaomei Fu
Chengdu University of Traditional Chinese Medicine
Zhixing Cao
Chengdu University of Traditional Chinese Medicine
Jinming Zhang (cdutcmzjm@126.com)
Chengdu University of Traditional Chinese Medicine https://orcid.org/0000-0002-4078-9048

Research

Keywords: Triptolide, nanoparticles, breast cancer, lung metastasis, low toxicity

Posted Date: March 16th, 2021

DOI: https://doi.org/10.21203/rs.3.rs-295313/v1

Abstract

Background

The toxicity and inefficient delivery of triptolide (TPL) in tumor therapy have greatly limited its clinical application. Therefore, we fabricated a CD44-targeting and tumor-microenvironment pH/redox sensitive nanosystem, composed by hyaluronic acid-Vitamin E succinate (HA-VE) and Poly (β-Amino Esters) (PBAEss) polymers, to enhance the suppression of breast cancer proliferation and lung metastasis of TPL.

Results

The generated TPL/NPs had the high drug loading efficiency (94.93 ± 2.1%) and a desirable average size (191 nm). Mediated by PBAEss core, TPL/NPs displayed a pH/redox dual stimuli drug release profile *in vitro*. Based on HA coating, TPL/NPs exhibited selective tumor-cellular uptake and high tumor-tissue accumulation capacity *via* targeting CD44. As a consequence, TPL/NPs showed higher cell proliferation suppression, pro-apoptosis and cell cycle arrest activities, and stronger inhibitory effects on cell migration and invasion than free TPL in MCF-7 and MDA-MB-231 cells. Importantly, TPL/NPs also showed higher efficacy in shrinking tumor size and block lung metastasis in a 4T1 breast cancer mice model at equivalent or lower TPL dosage compared to free TPL, with the decreased systemic toxicity. Histological immunofluorescence and immunohistochemical analyses in tumor and lung tissue revealed that TPL/NPs induced a high level of apoptosis, suppressed expression of matrix metalloproteinases, which all these contributed to inhibit tumor growth and pulmonary metastasis.

Conclusion

Collectively, our results demonstrate that TPL/NPs, which integrates tumor active-targeting and pH/redox responsive drug release, pro-apoptosis, and anti-mobility, represent a promising candidate in halting breast cancer progression and metastasis while minimizing systemic toxicity.

1. Introduction

Breast cancer remains one of the high-morbidity malignant tumors worldwide and the leading lethal cancer among females nowadays [1]. Rapid tumor growth and fast metastasis is the predominant death cause in breast cancer patients, in which the median 5-year survival rate is just about 26% [2]. Despite many clinical strategies including surgery, radio-therapy, and chemotherapy, have been used to attempt to eliminate tumor and inhibit metastatic spread of tumor currently, the treatment efficacy is still limited and the overall survival can only improve for a few months at most [3]. Particularly, the poor therapeutic outcome of chemotherapy, as the most mainstream treatment approach, attributes to the insufficient delivery efficiency to tumor site and/or the anti-metastasis ability of anticancer agent.

Triptolide (TPL) is a natural compound isolated from a Chinese medicinal herb *Tripterygium wilfordii*. Hook F.. Because of its various biological activity, it has attracted extensive attention in the medicinal field. Particularly, TPL processes substantial anti-cancer effects against a wide range of cancers [4, 5] with several signaling pathways involved, including the cell proliferation inhibition, cell apoptosis, and tumor metastasis suppression [6]. However, in spite of these anticancer benefits, several challenges, including the well acknowledged high toxicity [7], poor solubility, as well as the limited drug delivery efficiency to tumor site, still need to confront, which have severely impeded the potential clinical value of TPL. Recently, some strategies have been developed the TPL-targeted delivery systems [8], including to directly conjugate TPL with the selected targeting ligands [9, 10], and to encapsulate TPL in well-designed nano-vehicle.

However, in comparison with the instability of drug-ligand conjugation during transportation in the bloodstream, drugs loaded in nano-systems exhibit higher stability, long-circulating capacity, and higher accumulation efficiency in tumor site by EPR effect. Currently, multiple experimental evidence showed that the interaction of hyaluronic acid (HA) and CD44 receptor played an important role in cancer cell proliferation and migration, inflammation and tumor growth [11]. Many kinds of HA-modified/coating nanocarriers have been investigated to target CD44-overexpressing cancer cells, taking advantage of this interaction [12]. Moreover, these encapsulated drugs in nanoparticles with a stable core-shell structure urgently need to produce drug burst in cancer site selectively triggered by internal or external stimuli, while the scarce drug leakage in blood circulation [13]. In consideration of unique pathophysiology of tumors, it has been well reported to exhibit the acidic pH values in either tumor tissue (~ 6.5) or late endosomes/lysosomes (< 5.5). Poly (β-amino ester) (PBAE) is a cationic charged biodegradable polymer, which has been widely applied as biodegradable and biocompatible materials for anticancer drug delivery. Meanwhile, the rapid protonation of amino groups in PBAEs frameworks upon acidic pH can induce “proton sponge” effects of PBAEs-based nanoparticles, which facilitates the escape of encapsulated drugs from lysosomes [14, 15]. Additionally, redox-responsive nanoparticles also have aroused great enthusiasm of researchers due to the high intracellular concentration of glutathione (GSH) (approximately 2 ~ 10 mM) in tumor as compared to the extracellular environment (2 ~ 20 μM) [16]. Some pH- [17] or redox- [18] responsive nanoparticles loading TPL have been reported to benefit TPL’s delivery with the enhanced antitumor effects and reduced toxicity on normal tissues. Nevertheless, the nanocarriers with dual- or multiple- stimuli responsive characters would exhibit more sensitive and complete drug release than that with the single sensitive mechanism.

As a proof of concept, herein we designed a novel multifunctional nano-sized system with the tumor active-targeting and pH/redox dual-stimuli responsive properties to encapsulate TPL for the enhanced anti-breast cancer growth and metastasis. Specifically, a novel disulfide-containing poly(β-amino ester) (PBAEss) copolymer was synthesized in response to both pH and redox dual triggers, and acted as the hydrophobic core to load TPL. And then, Vitamin E succinate as a hydrophobic side chain was conjugated with HA to generate an amphiphilic copolymer (HA-VE), which would produce a shell coating on PBAEss nanocores. In that way, TPL loaded in this multifunctional nano-system (TPL/NPs) composed by HA-VE and PBAEss copolymers would facilitate to accumulate in tumor site through the EPR effect

and then be internalized into CD44 receptor over-expressing breast cancer cells mediated by HA-CD44 binding [19]. Subsequently, both the acidic pH of endosomes and high GSH in cytoplasm will accelerate the rapid escape of TPL from HA-VE/PBAEss NPs mediated by the “proton sponge” effect and disulfide bonds cleavage of PBAEss nanocore. Ultimately, these rapid accumulated TPL in tumor site benefit to induce cancer cell apoptosis and suppress the lung metastasis.

2. Results

2.1. Copolymer synthesis and characterization

VE was conveniently conjugated to HA with an esterification reaction via one synthesis steps in the presence of EDC and DMAP, as demonstrated in Fig. 1A. The synthesis of HA-VE conjugate was confirmed by ^{1}H NMR analysis. As shown in Fig. 1B, the characteristic peaks for methylene groups at the sugar unit and *N*-acetyl group of HA were identified at 3.10 ~ 4.00 ppm and about 1.80 ppm [20]. Intense peaks appeared at 0.8 ppm and 1.00 ~ 2.00 ppm represented the methyl group and methylene on fatty acid chain of VE [21]. These characteristic peaks could be observed in the ^{1}H NMR of HA-VE conjugate, indicating that it was successfully synthesized.

PBAEss were synthesized with the yield of 72.3%, mediated by Michael addition reaction as shown in Fig. 1C. The molecular weight of PBAEss copolymer was determined by gel permeation chromatography (GPC) analysis (Fig. S1). The Mw and Mn of PBAEss was 3.51×10^4 and 1.75×10^4, respectively (Mw/Mn = 2.00). The chemical structures of these intermediates, including 4-amino-1-butanol, HDD and BACy, and the synthesized PBAEss copolymer were characterized by ^{1}H NMR spectra (Fig. 1D). As shown, the characteristic peaks at 4.2 ppm and 5.5 ~ 6.5 ppm in HDD spectrum attributed to $-OCH_2-$ and vinyl protons. In BACy spectrum, the peaks at around 3.40 ppm and 5.5 ~ 6.5 ppm were assigned to the proton shifts of $-SCH_2-$ and the characteristic protons of vinyl protons, respectively. However, after polymerization between the vinyl of HDD and BACy, and amine group of 4-amino-1-butanol, the chemical shift derived from vinyl protons were disappeared in PBAEss spectrum. Meanwhile, the characteristic methylene proton peaks of NH_2CH_2-, $-CH_2-CH_2-$, and $-CH_2OH$ in 4-amino-1-butanol appeared respectively at 2.46 ppm, 1.2 ~ 1.5 ppm, and 3.4 ppm also could be found in the ^{1}H NMR spectrum of PBAEss. Altogether, the above results indicated PBAEss was successfully synthesized.

2.2. Preparation and characterization of TPL/NPs

PBAEss analogues have been previously demonstrated to form NPs for efficiently encapsulating genes or anticancer drugs by self-assembly based on its amphiphilic property. Herein, we encapsulated TPL into PBAEss nanocore using the nanoprecipitation method. Meanwhile, the hydrophilic HA-VE shell was coated on PBAEss nanocore by electrical charge interaction. To obtain the NPs with high drug loading efficiency and suitable size distribution, different compositions of HA-VE and PBAEss copolymer were utilized (Table S1). Conclusively, HA-VE, PBAEss, TPL with the amount of 10 mg, 10 mg, and 2 mg were feed. The collected TPL-loaded in HA-VE/PBAEss NPs (TPL/NPs) exhibited an average diameter of

approximately 191 nm with a relatively narrow distribution (Table 1). The drug loading efficiency (DLE) and drug entrapment efficiency (DEE) of TPL loading in NPs were determined as 8.63 ± 0.72% and 94.93 ± 2.1%, respectively.

The size distribution of TPL/NPs by dynamic light scattering (DLS) and morphology by Transmission Electron Microscopy (TEM) observation were shown in Fig. 2A. As shown, TPL/NPs had a uniform size distribution, regularly spherical shape and a compact structure. However, in response to either reductive (GSH 10 mM) or acid condition (pH 5.8) to mimic the redox and acid tumor microenvironment, the size distribution of TPL/NPs began to increase with multiple peaks. The uniform orbicular morphology of TPL/NPs changed into dispersion and fragment. The size changes of TPL/NPs in response to different conditions were shown in Fig. S2. These above results demonstrate that the TPL/NPs with the high drug loading and narrow particle size possessed the pH- and redox- dual responsive properties, which was suitable for the controlled release profiles in tumor microenvironment. Moreover, as depicted in Fig. S3, TPL/NPs could remain a stable particle size below 200 nm either in pH 7.4 PBS or in 10% serum supplemented DMEM at 4°C until 96 h place. After the continuous storage for 14 d, TPL/NPs exhibited the stable size distribution, with the RSD values of average size of 3.3% (Fig. S4). These results indicated the good stability of TPL/NPs, attributed to the uniform size distribution and anionic-based electrostatic repulsion.

To evaluate the intermolecular interaction between TPL and HA-VE/PBAEss nano-vehicle, fourier transform infrared spectroscopy (FT-IR) and X-ray diffraction (XRD) were employed. In Fig. 2B, the strong characteristic peak at 3455 cm^{-1} and 1770 cm^{-1} were shown in the FT-IR spectrum of TPL (a), derived from the hydroxyl group and carbonyl group in lactonic ring, respectively. Mediated by none of interference on these signals in FT-IR spectrum of blank NPs (b), the disappearance of these peaks in TPL/NPs (c) on the same chemical shift suggested that TPL was totally encapsulated in polymeric NPs, instead of physical mixture. Additionally, in the XRD spectrum (Fig. 2C), due to the crystal structure of TPL, the characteristic crystallization peaks mainly arranged at the range of 10°~40°. After loading in NPs, TPL/NPs transformed into amorphous form, indicating that there were no crystalline peaks in TPL/NPs.

To ensure the biosafety of TPL/NPs for intravenous injection, hemolysis analysis experiment was also conducted. We examined the effect of TPL/NPs on the hemolytic profile of RBC. PBS and water were used as the negative and positive control. As expected, the TPL/NPs with 1 ~ 50 μg/ml would not drive erythrocytes to release hemoglobin with a hemolysis rate of ≤ 5% (Fig. 2D). It indicated the safety of TPL/NPs and its compatibility for I.V. administration.

Table 1
Characterization of TPL/NPs

Samples	Particle size (nm)	PDI[a]	Zeta potential (mV)	DLE (%)	DEE (%)
Blank NPs	184.53 ± 7.52	0.195 ± 0.052	-6.33 ± 0.32	-	-
TPL/NPs	191.31 ± 7.08	0.176 ± 0.040	-6.94 ± 0.58	8.63 ± 0.72	94.93 ± 2.1

[a] Polydispersity index

2.3. *In vitro* drug release of TPL from TPL/NPs

In view of the pH/redox sensitive properties demonstrated by size changes above, the *in vitro* TPL release profiles from TPL/NPs under different mediums were measured using dialysis method, including the physiological condition (pH 7.4), only redox condition (pH 7.4, 10 mM GSH), only acid condition (pH 5.8), simulative tumor intracellular condition (pH 5.8, 10 mM GSH). Free TPL could be released rapidly as control, in which the cumulative release of TPL could reach about 90% of TPL during 8 h (Fig. 2E). At pH 7.4, TPL in NPs was released gently, only 45% of TPL was released from NPs druing 24 h, indicated the TPL molecules could be protected well in the core of HA-VE/PBAEss NPs. In comparison, TPL/NPs in response to either 10 mM GSH or pH 5.8 buffer exhibited much faster drug release, compared to that in pH 7.4 buffer. In response to 10 mM GSH, the PBAEss copolymer was expected to fracture due to the cleavage of disulfide bond. And when the pH value was decreased to 5.8, the drug release rate was sharply accelerated due to the protonation of tertiary amine residues in PBAEss segment. Therefore, the cumulative release of TPL for 24 h was 71.65% and 76.31%, respectively, indicated the intense initial burst release. At pH 5.8 with 10 mM GSH, the cleavage of disulfide bond and protonation of tertiary amine were combined, so that the drug release exhibited the fastest profile. The cumulative release of TPL reached to 85.32% during 24 h. Taken together, TPL-loaded in HA-VE/PBAEss NPs can efficiently exhibit a controlled release in physiological condition and a selectively rapid drug release in tumor microenvironment.

2.4. Cytotoxicity against breast cancer cells of TPL/NPs

After 48 h incubation, we investigated *in vitro* cytotoxicity of TPL/NPs in different media, i.e., pH 7.4, pH 7.4 + 10 mM GSH, pH 5.8, pH 5.8 + 10 mM GSH, respectively, against MDA-MB-231 and MCF-7 cells by MTT assay. The pH 5.8 value and 10 mM GSH of culture medium were characterized as the early endosome and cytoplasm of cancer cells. All these TPL formulas suppressed proliferation of MDA-MB-231 and MCF-7 cells in a dose-dependent manner at the range of 0 ~ 160 nM, whereas Blank NPs without TPL loading will not induce the cell viability reduction (Fig. 3, Fig. S5). Under the media of pH 7.4, TPL/NPs exhibited slightly higher cellular proliferation inhibition than free TPL, the IC_{50} values of TPL/NPs in both MDA-MB-231 and MCF-7 cells were close to that of free TPL. However, TPL/NPs showed much higher cytotoxicity at all concentrations of TPL exposed to these other culture media. Specifically, the average IC_{50} value of TPL/NPs in MCF-7 and MDA-MB-231 cells under pH 7.4 medium was 58.67 nM and 72.28 nM, while it remarkably reduced into 20.76 nM and 41.77 nM under the media

of pH 7.4 + 10 mM GSH ,reduced into 18.11 nM and 34.14 nM under the media of pH 5.8. Nevertheless, the IC_{50} values of TPL/NPs under the medium of pH 5.8 + 10 mM GSH were minimum, which sharply decreased into 13.77 nM and 26.39 nM in MCF-7 and MDA-MB-231 cells, respectively (Fig. 3C). These results are well consistent with the *in vitro* drug release profile, indicated that the pH-/redox- sensitive NPs facilitate the drug release and efficiently kill the tumor cells.

2.5. TPL/NPs enhanced the cell apoptosis and cell cycle arrest

Apoptosis is the main mechanism accounting for the anticancer of TPL [22]. Herein, we further evaluated whether TPL/NPs would enhance the apoptosis in both MDA-MB-231 and MCF-7 cells. To thoroughly mimic the acid and reductive microenvironment in tumor, we performed the apoptosis induction of TPL/NPs under pH 7.4 without GSH or pH 5.8 with 10 mM GSH. Apoptosis was analyzed by annexin V-FITC / PI staining. As shown in Fig. 4, with the equivalent TPL amount of 20 nM for 24 h incubation of MDA-MB-231 cells, TPL/NPs at each condition exhibited higher apoptosis rate than free TPL. Especially, TPL/NPs in culture medium of pH 5.8 with 10 mM GSH induced the highest apoptosis rate, compared to other counterparts. The apoptosis rate of TPL/NPs at pH 5.8 with 10 mM GSH was 2 and 1.6 -fold of that of free TPL and TPL/NPs at pH 7.4, respectively. Moreover, the results in MCF-7 cells were also in accordance with that in MDA-MB-231 cells.

Cell cycle phase distribution was analyzed by flow cytometry (FCM) with PI staining, which could measure the cellular DNA content. As shown in Fig. 5, after 24 h incubation in MDA-MB-231 cells with 10 nM TPL, a high proportion of cells in Sub-G_0/G_1 was observed, which indicated the occurrence of cell apoptosis. It was in accordance with the previous report about the $SubG_1$ phase arrest of TPL [23]. Meanwhile, more either MCF-7 or MDA-MB-231 cells were significantly arrested in G_0/G_1 phase when treated with TPL/NPs, compared to that treated with free TPL. As expected, the TPL/NPs in the medium of pH 5.8 + 10 mM GSH also induced a significantly higher G_0/G_1 population than that in the medium of pH 7.4.

In summary, TPL/NPs exhibited the stronger pro-apoptosis and G_0/G_1 cell cycle arrest capacity in both MDA-MB-231 and MCF-7 cells compared to free TPL. In view of the stimuli-responsive drug release of TPL/NPs, both the cell apoptosis and cell cycle arrest of TPL/NPs exhibited the significant enhancement in response to pH-/redox- culture medium, suggesting that TPL/NPs benefited to play its anticancer effect in tumor microenvironment.

2.6. Cellular uptake study

To determine whether the TPL/NPs specifically enhanced cellular uptake of breast cancer cells, we measured the uptake of C6/NPs in MDA-MB-231 and MCF-7 cells after being treated for 1, 2, and 4 h by FCM. After incubation with free C6 and C6/NPs, the accumulation of free C6 and C6/NPs in MDA-MB-231 and MCF-7 cells was time-dependent (Fig. 6A and 6B). Besides, after co-incubation with cells, cellular

uptake of C6/NPs was significantly greater than that of free C6 at different time intervals, indicating enhanced cellular uptake of nanosize agents. The enhanced cellular uptake of C6/NPs was mediated by active transport in an energy dependent manner (Fig. S6A), rather than the passive diffusion of free hydrophobic C6. Additionally, drugs loading in NPs could avoid being easily pumped out from cells.

Besides, we also observed the cellular uptake of C6/NPs both in MDA-MB-231 and MCF-7 cells by confocal laser scanning microscopy (CLSM) (Fig. 6C and 6D). After treatment for 4 h, higher cellular internalization of C6 was found in cells treated with C6/NPs than in cells treated with free C6. These data were consistent with FCM results, indicating that C6/NPs were effectively taken up.

2.7. Competitive uptake study

To investigate the CD44-targeted delivery of the TPL/NPs, CD44-positve MDA-MB-231 breast cancer cell line and CD44-negative MCF-7 epithelial cell line were chosen (Fig. S7)[24]. Figure 6C and 6D taken by CLSM showed the intracellular uptake of C6/NPs in CD44-positive MDA-MB-231 cells and CD44-negative MCF-7 cells. The cell nuclei was stained with Hoechst 33342, which exhibited strong blue fluorescence. Compared to free C6 group, we observed a more intense fluorescence signal in MDA-MB-231 and MCF-7 cells when incubated with C6/NPs. However, when C6/NPs group was pretreated with free HA for 1 h (C6/NPs + HA), the fluorescence expression was significantly decreased in MDA-MB-231 cells, which indicated that free HA blocked the CD44 receptor on the surface of MDA-MB-231 cells and inhibited internalization of C6/NPs. On the other hand, when C6/NPs group was pretreated with 5 mg/ml of free HA for 1 h (C6/NPs + HA), the fluorescence expression was slight reduced in MCF-7 cells. The results indicated that HA-modified NPs could specifically bind to the CD44 receptor on the surface of tumor cells and promote cellular uptake by active targeting.

Furthermore, the competitive study was studied in CD44 high-expressed MDA-MB-231 cells by FCM. The cells were pretreated with free HA followed by incubated with C6/NPs. The result is shown in Fig. S6B where the cellular accumulation of C6/NPs was reduced to 48.58 ± 3.7%. It demonstrated that the cellular uptake of C6/NPs was contributed to HA polymer specific binding to CD44 receptors. The free HA competed with HA-conjugated NPs for CD44 receptors and inhibited cellular uptake of HA-conjugated NPs in cells.

2.8. Endocytosis pathway

We utilized different endocytic inhibitors to identify the possible endocytotic pathways involved in the uptake of TPL/NPs, including chlorpromazine (clathrin-mediated), indomethacin (caveolae-mediated), methyl-β-cyclodextrin (cholesterol-dependent endocytosis) and colchicine (macropinocytosis inhibitor) [25]. As shown in Fig. 6E, the internalization of C6/NPs was significantly decreased by the pretreatment of indomethacin or methyl-β-cyclodextrin, indicating the process of internalization of C6/NPs was involved in caveolae-mediated and cholesterol-dependent endocytosis. In contrast, the pretreatment of neither chlorpromazine nor colchicine could exert little effect on cellular uptake of C6/NPs, excluding the involvement of clathrin-mediated endocytosis and macropinocytosis.

2.9. TPL/NPs inhibited MDA-MB-231 cell migration and invasion

The MDA-MB-231 cell line as the triple negative breast cancer cell possesses high metastatic character [26]. We conducted wound-healing assay to evaluate whether the TPL/NPs treatment could suppress the migration of MDA-MB-231 cells. The results indicated that the wound gaps in the TPL/NPs-treated groups were significantly wider than either those of the untreated groups or those of free TPL treatment group, indicated that TPL/NPs could more effectively inhibit the migration of MDA-MB-231 cells compared to free TPL (Fig. 7A and 7B). Particularly, in the medium of pH 5.8 with 10 mM GSH, the migration inhibition of TPL/NPs was remarkably higher than other counterpart.

Furthermore, the anti-metastasis effect of TPL/NPs was evaluated by transwell experiments. Consistent with the results of the wound healing assay, TPL/NPs effectively suppressed cell migration. Only a few MDA-MB-231 cells migrated from the upper chamber to the lower chamber of the transwell following the treatment with TPL/NPs in pH 5.8 + 10 mM GSH, indicated that TPL/NPs significantly inhibited the longitudinal motility of MDA-MB-231 cells (Fig. 7C and 7D).

To study the effect of TPL/NPs on cell invasion, MDA-MB-231 cells were treated with either free TPL or TPL/NPs, then allowing cells to invade in Matrigel-coated Transwells for 24 h. The number of cells that invaded was decreased by various TPL formulas (Fig. 7C and 7E). Compared to the untreated group, free TPL, TPL/NPs in pH 7.4, and TPL/NPs in pH 5.8 + 10 mM GSH inhibited invasion by ~ 45%, 52%, and 67%, respectively. The results clearly demonstrated that TPL/NPs could strongly suppress MDA-MB-231 cell migration and invasion, with the pH-/redox- dual sensitive combination effects. These above results implied the anti-metastasis potential of TPL/NPs.

2.10. *In vivo* biodistribution of HA-VE/PBAEss NPs

The tumor targeting capacity of HA-VE/PBAEss NPs was further investigated in 4T1 tumor bearing nude mice. To label the HA-VE/PBAEss NPs with fluorescence, DiR was firstly encapsulated into NPs with the similar approach as TPL as shown in Fig. 8A. When the tumor volume reached about 1000 mm^3, the mice were administrated intravenously with free DiR and DiR/NPs. The mice were imaged using the IVIS® Spectrum scanner during 72 h post-injection (Fig. 8B). At 72 h, the mice were sacrificed, and the main organs as well as tumor were harvested and visualized *ex vivo* (Fig. 8C). As shown, after administration of free DiR by *i.v.*, the NIR fluorescence *in vivo* attenuated sharply, and few of fluorescence could be found in tumor tissue, indicated that the rapid body clearance and poor tumor accumulation capacity. However, much more fluorescence with a prolonged period can be found in mice treated with DiR/NPs. Particularly, the significant tumor accumulation of DiR/NPs could be observed. Even after 72 h post-injection, strong fluorescence still could be found in tumor tissue. After injection of DiR/NPs for 72 h, the strong signal can be observed in tumor, instead of the unconspicuous fluorescence of tumor in free DiR group. This indicated that the tumor accumulation of vesicles composed by HA-VE/PBAEss copolymers, which would attribute to the prolonged circulation, EPR effect and tumor targeting mediated by HA and CD44

interaction. Taken together, the results indicated that the *in vivo* long-circulation and tumor accumulation of TPL can be efficiently enhanced by the capsulation of HA-VE/PBAEss NPs.

2.11. Inhibition of primary tumor growth and metastasis in vivo

Mediated by the combination of tumor-homing properties and dual stimuli-triggered tumor release profiles of TPL/NPs, we assumed that it could be much more efficient in chemotherapy. Therefore, we established a 4T1 subcutaneous tumor bearing mouse model to further evaluate the *in vivo* efficacy in suppressing primary tumor growth and distant metastasis. After treated with different administrations for 20 days, the tumor growth curves (Fig. 9A) and body weight (Fig. 9B) were presented, which were measured every two days. As shown, the blank HA-VE/PBAEss NPs shown no distraction on tumor growth as well as body weight, similar to saline control group. However, mice treated with TPL formulations exhibited better antitumor activity, compared to saline group. The tumor volume inhibition rates for TPL, TPL/NPs (L) and TPL/NPs (H) were 54.86%, 70.10%, and 84.76%, respectively. Particularly, the TPL/NPs at either 0.2 mg/kg or 0.4 mg/kg exhibited higher tumor growth inhibition efficacy than free TPL at 0.4 mg/kg. The TPL/NPs (H) almost inhibited the bearing tumor tissue growth completely. Meanwhile, after a successive administration of free TPL for 14 days, mice exhibited the declined body weight, indicated the potential side-effects. Nevertheless, after loading in NPs, TPL exhibited the higher biosafety. The differences among groups on inhibition effects to primary tumor can be directly observed in Fig. 9C. At the experimental end point, tumor weight in each group had the same trend with the result of tumor volume (Fig. 9D). These results demonstrated that TPL/NPs (H) with the TPL of 0.4 mg/kg possessed the best curative effect on primary tumor and non-side effects.

The 4T1 subcutaneous tumor has been demonstrated to be prone to induce pulmonary metastasis. In view of the cell migration and invasion inhibition effects *in vitro*, the anti-metastasis ability of TPL/NPs *in vivo* was also evaluated. After perfusing the lungs with ink gelatin solution, the pulmonary metastatic nodules could be visible. A large number of metastatic nodules were observed in the lungs of the saline and blank NPs groups (Fig. 9E). Compared with the saline group, the number of pulmonary metastatic nodules in mice treated with TPL, TPL/NPs (L) and TPL/NPs (H) decreased by 55.38%, 67.70%, and 89.99%, respectively (Fig. 9F). The number of pulmonary metastatic nodules in TPL/NPs (H) group were remarkably less, compared to other counterparts. These results corroborated that TPL/NPs could efficiently suppress primary tumor growth and pulmonary metastasis.

2.12. Potential anti-tumor and anti-metastasis mechanisms

To further investigate the mechanisms of proliferation and metastasis inhibition of TPL/NPs *in vivo*, the tumor tissues were implemented by hematoxylin and eosin (H&E) and immunohistochemical staining (Fig. 10A). The H&E images indicated that the TPL/NPs induced the limited proliferation and severe apoptotic damages, even necrocytosis, in the tumor compared to either free TPL or blank NPs. This result was also confirmed by the immunohistochemical staining of Bcl-2 and Ki-67 antibody. In TPL/NPs (H) group, the number of brownish yellow points represented the positive cells was much fewer than other counterparts. In our previous study, we have demonstrated that TPL could significantly suppress the

angiogenesis, benefiting to block the tumor growth. Herein, the expression of CD31 was significantly downregulated in TPL/NPs (H) group compared with other groups, indicated the higher anti-angiogenesis activity of TPL/NPs. Moreover, the expression of MMP-9 in the tumor tissue possesses a close relationship with tumor invasion and metastasis. As shown, the expression of MMP-9 was uniform over the whole slice of saline group, while the lowest expression of MMP-9 was observed along with the treatment of TPL/NPs (H). E-cad as an important EMT-relative protein plays a pivotal role in many epithelial malignant tumors invasion and metastasis. Invasion of surrounding tissues and metastasis have been proposed to initiate following loss of E-cadherin (E-cad) [27]. As expected, low expression of E-cad could be found in saline group, while the remarkably increased E-cad expression appeared in the TPL/NPs (H) group. The downregulated MMP-9 and upregulated E-cad indicated that after treatment with TPL/NPs, the metastasis process was significantly restrained (Fig. 10B). The similar results were also observed in histological staining images of lung tissues by H&E and immunohistochemical staining (Fig. S8). Because of the generation of pulmonary metastatic nodules, the cell proliferation, blood vessel and cell migration in lung tissue of saline group exhibited extremely active. However, the treatment of TPL/NPs could effectively callback the abnormal upregulation on the expression of these representative proteins including Bcl-2, Ki-67, CD31, MMP-9, and the decreased E-cad amount in lung tissue. These results were consistent with the conclusion obtained from tumor tissue of immunohistochemical analysis.

Furthermore, to validate the regulation effect on tumor growth and metastasis of TPL/NPs, western blotting analysis was also performed to assess the expression of some apoptosis and metastasis signaling proteins, including p53, caspase 3, MMP-2, and vimentin. As shown in Fig. 10C and 10D, TPL/NPs significantly upregulated the protein levels of p53 and caspase 3, compared to either control group or free TPL group. Therefore, combined with the regulation of Bcl-2, caspase 3 and p53, the data demonstrated that TPL/NPs significantly induced tumor apoptosis mediated by mitochondrial apoptotic pathway. In addition, the representative proteins in tumor EMT process including MMP-2 and vimentin were evaluated by western blot. As expected, the levels of MMP-2 and vimentin were remarkably decreased in TPL/NPs groups (Fig. 10D). In view of the regulation of E-cad, MMP-9, MMP-2 and vimentin, the results shown that TPL/NPs effectively suppressed tumor metastatic effects *in vivo*.

Although the outstanding antitumor growth and anti-metastasis effect of TPL/NPs have been observed, whether TPL/NPs could result in the side-effect was still unclear, in view of the acknowledged severe side-effects of TPL. Therefore, we evaluated the histological images of the main organs by H&E staining and some blood biochemical indexes. Compared to saline group, free TPL-treated mice showed histopathological changes in liver tissue, characterized by fat vacuoles, inflammatory cell infiltration and necrosis (Fig. 11A). It indicated the liver injury caused by free TPL administration. However, the severity of histopathological lesions in TPL/NPs groups were less than those in the free TPL group. Furthermore, significant increases in alanine aminotransferase (ALT) and aspirate aminotransferase (AST) levels in blood were observed in mice serum treated with 0.4 mg/kg of the free TPL compared to saline group (Fig. 11B). In contrast, the administration of TPL/NPs with each dosage don’t lead to significant changes

in the levels of those indexes. However, there were no obvious differences in the levels of urea nitrogen (BUN) and creatinine (Cr) among all groups.

3. Discussion

Presently, surgery and chemotherapy are the main treatment methods for breast cancer. However, due to non-specificity to tumors and drug-related toxicity to non-targeted tissues and organs, the clinical efficacy of systemic therapy is usually affected. In addition, breast cancer metastasis is one of the main causes of cancer death in female patients. Thus, methods to improve the efficacy of chemotherapeutic drugs and overcome tumor metastasis could significantly improve the prognosis of breast cancer patients.

TPL has strong pharmacological effects, but its toxic effects on the organs including liver, kidney, skin, gastrointestinal tract, heart and reproductive system limit its therapeutic window [28]. In this study, we tried to reduce the toxicity of TPL and enhance its anti-tumor inhibition and metastasis activity. The TPL/NPs is a highly effective and low toxic tumor therapy, which could solve the systemic toxicity of TPL. This may be attributed to the enhancement of tumor accumulation and redox-responsive and pH-responsive targeted at the tumor part by HA targeting CD44.

Furthermore, our work demonstrated that the administration of both the free TPL and TPL/NPs efficiently reduced the expression levels of Bcl-2 and increased the expression levels of p53 and caspase 3, which are crucial proteins in the apoptosis signaling pathway. More interestingly, our data further demonstrated a stronger target regulation efficacy of the TPL/NPs compared to the free drug. On the other hand, as the most important marker for EMT, E-cad has been reported to be responsible for the intercellular connections and polarity [29]. As expected, the expression of E-cad was significantly upregulated in free TPL and TPL/NPs treated groups. In addition, TPL/NPs directly regulated EMT progression by decreasing vimentin expression. MMPs are a family of zinc-dependent endopeptidases, and are the main proteases that invade and degrade basement membranes and extracellular matrix. As previous study reported, inhibiting MMPs could significantly reduce invasiveness [30]. MMP-2 and MMP-9 are the key members of MMPs family, which can cleave gelatin, collagens, elastin and vitronectin, which are necessary for cell invasion and migration [31]. Our results shown that TPL/NPs inhibited the expression of MMP-2 and MMP-9. In summary, results above indicated that TPL/NPs could significantly inhibit cell apoptosis, proliferation and invasion, thereby exhibit an excellent anti-metastatic effect *in vivo*.

4. Conclusion

Herein, we developed a multiple functional nanocarrier, by the self-assembly of hyaluronic acid-Vitamin E succinate (HA-VE) and Poly(β-Amino Esters) (PBAEss) polymers, to enhance the tumor growth inhibition and lung metastasis effect of triptolide (TPL). This nanosystem possesses the integrated advantages including tumor targeting mediated by CD44 receptor, proton sponge effect in response to acidic endosome pH, GSH-responsive drug burst release, as well as the combined anticancer and anti-metastasis effect of TPL. *In vitro* cellular experiments confirmed the enhanced cellular proliferation

inhibition of TPL/NPs against both MCF-7 and MDA-MB-231 cells, which was related to the upregulation of cell apoptosis and cell cycle arrest. Additionally, TPL/NPs exhibited prominent anti-migration and anti-invasion activities in MDA-MB-231 cells, in view of its high mobility. Besides, because of the superior tumor accumulation capacity, TPL/NPs could efficiently inhibit the growth and lung metastasis of breast tumor, in the bearing 4T1 carcinoma xenograft mice model. Meanwhile, TPL/NPs showed lower systemic toxicities than free TPL. This work revealed that TPL/NPs represent a promising candidate in halting breast cancer progression and metastasis while minimizing systemic toxicity.

5. Materials And Methods

5.1. Chemicals and reagents

Triptolide (TPL) was obtained from Chengdu DeSiTe Biological Technology Co., Ltd. Hyaluronic acid (HA) (Molecular weight 8 kDa) was acquired from Freda Biochem Co., Ltd. (Shandong, China). 1,10-dioctadecyltetramethyl indotricarbocyanine iodide (DiR) was obtained from Mellon, Biological Technology co., Ltd. (Dalian, China). 4-amino-1-butanol, 1,6-hexanediol diacrylate (HDD) and N, N'-bis(acryloyl)cystamine (BACy) were purchased from Macklin Reagent Co. Ltd. (Shanghai, China). Vitamin E succinate (VE, purity ≥ 98%), 1-(3-Dimethylaminopropyl)-3-ethylcarbodiimide hydrochloride (EDC), 4-(dimethylamino)-pyridin (DMAP), Dimethyl sulfoxide (DMSO) and 3-(4,5-dimethylthiazol-2-yl)-2,5-diphenyltetrazoliumbromide (MTT) were obtained from Macklin Reagent Co. Ltd. (Shanghai, China). DMEM, fetal bovine serum (FBS), horse serum (HS), phosphate-buffered saline (PBS), penicillin-streptomycin, and 0.25% (w/v) trypsin containing 1 mM EDTA were purchased from Invitrogen (Carlsbad, CA, USA). FITC anti-human CD44 was purchased from 4A Biotech Co., Ltd. Other organic solvents or reagents were analytic grade and used as received.

5.2. Cell culture

MDA-MB-231, MCF-7 and 4T1 cells were purchased from American Type Culture Collection (Manassas, USA). PC-12 cells were obtained from Kunming Institute of Zoology (Kunming, China). DMEM containing 10% FBS and 1% penicillin-streptomycin was used to culture MDA-MB-231, MCF-7 and 4T1 breast cancer cells. DMEM supplemented with 10% HS, 5% FBS and 1% penicillin-streptomycin was used to culture PC-12 cells. All the cells were incubated at 37°C in a humidified atmosphere with 5% CO_2.

5.3. Animal feeding

Female BALB/c nude mice (4 weeks of age; 14–16 g) were obtained from SPF (Beijing) biotechnology co., Ltd. (Beijing, China) and fed in animal care facility for 12 h light/dark cycle. All animals were acclimated for at least 7 days before the experiments and were given a fresh diet and free drinking water.

Obtained the animal experiment ethics certification of Chengdu University of Traditional Chinese Medicine (CDUTCM, permit CDU2019S121).
All animal experiments were conducted in accordance with university guidelines.
Animal welfare was guaranteed in all animal experiments.

5.4. Synthesis of HA-VE and PBAEss copolymers

HA-VE conjugates were subsequently synthesized by an esterification reaction of HA with VE [32]. Briefly, VE (2 mmol) and EDC (3 mmol) were dissolved in 20 mL of anhydrous DMSO and stirred for 2 h to activate the carboxyl group. Next, add HA (2 mmol) and DMAP (2 mmol) into the mixture, continue to react at 30°C for 48 h with a magnetic stirring bar. Then, the HA-VE mixture was successively dialyzed against deionized water using a dialysis tube (MWCO 1000) for 2 d removing unreacted substance. The HA-VE was then lyophilized and stored at -20°C. The structure of HA-VE were characterized using ^{1}H NMR [33].

We used a Michael-type step polymerization to synthesize the PBAEss copolymer [33]. In brief, 4-amino-1-butanol (5 mmol), 1,6-hexanediol diacrylate (2.5 mmol) and BACy (2.5 mmol) were dissolved using 10 mL DMSO with continuous stirring for 24 h at 90°C. Then, using a dialysis bag (MWCO 5000) first in DMSO and subsequently in PBS (pH 7.4) to remove unreacted materials. Finally, PBAEss was obtained after freeze-drying and stored at -20°C. ^{1}H NMR was used to characterize the structure of PBAEss and GPC was used to measure the molecular weights of the synthesized PBAEss copolymers [34].

5.5. Preparation and characterization of TPL/NPs

TPL encapsulated in TPL/NPs composed by HA-VE and PBAEss copolymers (TPL/NPs) was prepared by nanoprecipitation method. In short, PBAEss and TPL were dissolved in 2 mL of methanol and assisted in sonication dispersion at the power of 90 W for 60 s. Then, HA-VE was dissolved in 10 mL of PBS (pH 7.4) with mild stirring for 5 min. The mixture of organic solvent (containing TPL and PBAEss) was then dropped in aqueous phase (PBS (pH 7.4) containing HA-VE) with a stirring for 4 h at 30˚C to evaporate the residual methanol. Finally, we used 0.45 μm micro-porous membrane to remove free TPL drugs. The obtained TPL/NPs sample was stored at 4°C.

The characterization of TPL/NPs including size distribution, surface charge, morphology, drug loading capacity, drug release, stability, hemolytic and serum stability were implemented based on the previous studies and descripted in the Supplementary Material.

5.6. Redox and pH-responsive capability of TPL/NPs

The TPL/NPs were dispersed in PBS (pH 7.4) with 10 mM of GSH over 24 h or within acidic environments of pH 5.8 over 24 h at a final diluted material concentration of 1 mg/mL under stirring at 100 rpm, respectively. After designated time intervals (0, 2, 4, 6 and 24 h), the mean particle sizes of the TPL/NPs were measured by a Zetasizer Nano ZS 90. Meanwhile, the morphology changes of TPL/NPs in response to either acid buffer (pH 5.8) or reductive buffer (10 mM GSH) were exhibited mediated by TEM observation.

5.7. Cytotoxicity of TPL/NPs against breast cancer cells

MDA-MB-231 and MCF-7 human breast cells were seeded into 96-well plates at a density of 3×10^3 cells/well for 24 h [35]. And then MDA-MB-231 and MCF-7 cells were given free TPL, Blank NPs and TPL/NPs with various concentrations (0 ~ 160 nmol/L) in different culture media (pH 7.4, pH 7.4 + 10 mM GSH, pH 5.8, pH 5.8 + 10 mM GSH) for 48 h, respectively. Cells treated with 0.1% DMSO served as negative control. According to the manufacturer's protocol, the MTT assay was used to measure cell viability.

5.8. Apoptosis analysis by FCM

Cell apoptosis induced by various TPL formulas was detected by an Annexin V-FITC/PI detection kit (Biovision, USA). MDA-MB-231 and MCF-7 cells (6×10^4 cells/well) were seeded in 6-well plates and then treated with free TPL, and TPL/NPs with the equivalent concentrations of TPL at 20 nM in different media (pH 7.4, pH 5.8 + 10 mM GSH, respectively) for 24 h. Cells were harvested with EDTA-free trypsin and stained with Annexin V-FITC and PI according to the manufacturer's instructions of Apoptosis Kit. Finally, each sample was analyzed by using FCM (BD Biosciences, California, USA).

5.9. Cell cycle analysis

The seeded MDA-MB-231 and MCF-7 cells (5×10^4 cells/well) were cultured in FBS free medium for 24 h for cell cycle synchronization. And then, cells were treated with free TPL and TPL/NPs with the equivalent concentrations of TPL at 10 nM in different media (pH 7.4, pH 5.8 + 10 mM GSH, respectively) for 24 h. The cells were trypsinized and washed with PBS. Next, fixed the cells in cold 70% ethanol at 4°C for 24 h. The cells were collected by centrifugation and stained with 5 μL of PI solution (Life Technologies, USA) for 10 min. The cell samples were run using FCM, and the cell distribution of single cell suspension was analyzed using FlowJo V10 software (version 3.0, USA).

5.10. Cellular uptake study

To take advantage of the HA-CD44 interaction mediated intracellular uptake, the expression level of CD44 receptors in MDA-MB-231, MCF-7, and P12 cells, which represented as the high, low and scarce expression of CD44 receptors, were detected by the immunofluorescence method with the detailed description in Supplementary Material.

Owe to the positive expression of CD44 receptor in MDA-MB-231 and MCF-7 cells, the cellular uptake of HA-VE/PBAEss NPs in cells was determined quantitatively and qualitatively respectively. Coumarin 6 (C6) was primarily loaded in HA-VE/PBAEss NPs based on the similar preparation approach as the fluorescent label. And then C6/NPs were co-cultured with MDA-MB-231 and MCF-7 cells respectively to investigate the cellular uptake behavior of NPs. In brief, MDA-MB-231 and MCF-7 cells were respectively seeded into the six-well plate at a density of 2×10^5 cells/well for 24 h adherence. Then, the culture medium was replaced into serum-free fresh medium containing free C6 or C6/NPs with the equivalent C6 concentration of 100 ng/ml. After incubation for 1 h, 2 h and 4 h, respectively, the medium was removed and the cells were washed with cold PBS. Cells were collected by trypsin and re-suspended in PBS for FCM assay. The data presented were based on the mean fluorescence signal for 10,000 cells collected.

Additionally, the CLSM was used to present the cellular uptake of NPs. MDA-MB-231 and MCF-7 cells were firstly seeded into 35 mm glass bottom dishes for 24 h. And then, cells were incubated with free C6, and C6/NPs with the equivalent C6 concentration of 100 ng/ml for 4 h. Finally, cells were washed with PBS and fixed in cold 4% paraformaldehyde for 10 min. The cell nuclei were stained with Hoechst 33342 for 10 min and then observed by CLSM.

Due to the high expression of CD44 receptor in MDA-MB-231 cells, the intracellular mechanisms of HA-VE/PBAEss NPs in MDA-MB-231 cells were evaluated mediated by some endocytosis inhibitors. Likewise, MDA-MB-231 cells were cultured in six-well plates at a density of 2×10^6 cells/well. After overnight incubation, 1 mL medium containing some inhibitor agents including 10 μg/ml chlorpromazine, 6 μg/ml indomethacin, 8 μg/ml colchicine, 5 mM methyl-β-cyclodextrin, and 5 mg/ml HA was used to replace the original medium for 1 h. And then, C6/NPs with the C6 concentration of 100 ng/ml were co-cultured with cells for another 4 h. The intracellular profiles of fluorescence probe were determined by CLSM and FCM respectively as above descripted.

5.11. Wound healing assay

MDA-MB-231 cells were seeded into the six-well plate and cultured to 80%~100% confluence. Then carefully damage the cell monolayers with a sterile toothpick and wash with PBS for three times. After that, the wounded cell monolayers were treated with free TPL or TPL/NPs (5 nM) for 24 h. The control group was only given the medium solution for the same time. The wounds were established by carefully scratching the confluent cells by a 200 μL pipet tip. Observe the distribution of the cells at the scratch zone using a microscope obtained images. The scratch area was obtained by ImageJ software, and the percentage of wound closure was evaluated as the parameter of wound closure degree.

5.12. Transwell migration and invasion assay

Cell migration and invasion assays in MDA-MB-231 cells were performed using a 24-well Transwell chamber as described previously [36]. The upper and lower sides of the Transwell membrane (8 μm pores) were pre-coated with 0.1% collagen in the cell migration assay. Compared to the cell migration assay, the upper and lower sides of the membrane were pre-coated with 100 μL matrigel (20% in blank medium) in the cell invasion assay. Briefly, MDA-MB-231 cells were seeded into the Transwells at a density of 5×10^4 cells/well with low serum medium. Cells were treated with free TPL or TPL/NPs for 24 h at 37°C, and the cells on the upper surface of the Transwell membrane were then removed using cotton swabs. Next, the Transwell membranes were fixed with 4% paraformaldehyde for 15 min, and stained with Hoechst 33342 (10 μg/mL) for 15 min. Finally, the membranes were mounted on microscope slides and images were captured using a fluorescence inverted microscope and a charge-coupled device camera (AxioCam HRC, Carl Zeiss, Oberkochen, Germany). Cell migration and invasion were quantified by counting the number of cells per insert using ImageJ software (National Institutes of Health, Bethesda, USA).

5.13. Tumor accumulation imaging in vivo and ex vivo

The tumor accumulation profile of NPs was greatly related to the tumor suppression effects and toxicity on normal organs. In order to track the biodistribution of NPs *in vivo*, DiR, a near infrared fluorescence dye, was applied to replace TPL and loaded in NPs. Tumor-bearing mice were established by subcutaneous injection of 1×10^6 4T1 cells in 100 μl PBS containing 50% Matrigel on the right axilla of nude mice. When tumor volume reached approximately about 1000 mm^3, the tumor-bearing mice were randomly divided into two groups, including administrated by tail vein injection of free DiR and DiR/NPs (with the equivalent DiR amount of 0.05 mg/kg). The images were purchased using Caliper LifeSciences LIVIS® Lumina Series (PerkinElmer, MA, USA) at the excitation wavelength of 745 nm and emission wavelength of 800 nm. At a series of time interval including 0, 0.5, 2, 4, 6, 12, 24, 36, 48 and 72 h post-injection, the fluorescence images were collected. At 72 h post-injection, the mice were sacrificed to obtain the tumor, heart, liver, spleen, lung and kidney. The data was analyzed using Living Image Version 4.5 software (PerkinElmer, MA, USA).

5.14. In vivo anti-tumor and anti-metastasis effect

The breast cancer model was established through subcutaneous flank inoculation of 1×10^6 4T1 cells in 100 μl PBS containing 50% Matrigel on BALB/c female mice. When the tumor volume reached 100 ~ 200 mm^3, the mice were treated with saline (control), Blank NPs, Free TPL (0.4 mg/kg), TPL/NPs (0.2 mg/kg, L) and TPL/NPs (0.4 mg/kg, H), respectively every other day, by tail vein injection (n = 6). Tumor size of mice was measured with calipers every other day and tumor volumes were calculated according to the formula $V = length\times width^2/2$. The body weights of mice were monitored during the whole experimental period. After day 21, the mice were sacrificed through an overdose of anesthetic, and the tumors and the main organs (including heart, liver, spleen, lung, and kidney) of mice were obtained and photographed. The tumors and the main organs were weighed and fixed with 4% (v/v) formalin neutral buffer solution and sectioned into 6 μm slices. Additionally, the lung tissue was perfused with 15% Indian ink from trachea. The number of macroscopic metastatic nodules per lung was recorded to calculate the inhibitory effects on lung metastasis of breast cancer. Moreover, mice blood was centrifuged at 4°C for 10 min at 4,000 rpm. Serum was collected and stored at -20°C for analysis. The levels of blood AST, ALT, BUN and Cr were detected by blood biochemical analyzer.

The histopathology examinations of tumor and lung sections were performed by H&E staining. Meanwhile, these tissue sections were stained with primary antibodies against MMP-9, E-cad, CD31, Bcl-2 and Ki-67 (Abcam, Cambridge) to evaluate angiogenesis and cell proliferation in tumor and lung tissue. Quantification was done in a blind fashion by counting positive cells in 10 fields (200×) using a light microscope (Zeiss, Germany).

Moreover, the protein expression of p53, caspase 3, MMP-2 and vimentin in tumors were evaluated by western blot analysis. Tumor samples were collected and homogenized with the radio immunoprecipitation assay (RIPA) lysis buffer. The extracted protein samples were separated by 4%~12% sodium dodecyl sulfate polyacrylamide gel (SDS-PAGE) electrophoresis and transferred onto polyvinylidene difluoride (PVDF) membranes. The membranes were incubated with the indicated primary

antibodies including anti-p53 (1:1000), anti-caspase-3 (1:1000), anti-MMP-2, anti-vimentin (1:1000) and anti-GAPDH (1:2000) at 4 ℃ overnight. And then, membranes were incubated with a horseradish peroxidase-coupled secondary antibody, and signals were observed using the Pierce ECL Western Blotting Substrate (Thermo, Rockford, IL). The relative expression level of protein was quantified with ImageJ software.

5.15. Statistical analysis

Data are expressed as the mean ± SD of at least three independent experiments. Data were analyzed by GraphPad Prism 8.0 (La Jolla, CA, USA). Statistical significance was determined by one-way analysis of variance, and a P value of < 0.05 was considered significant.

Abbreviations

TPL: Triptolide; HA-VE: Hyaluronic acid-Vitamin E succinate; PBAEss: Poly (β-Amino Esters); GSH: Glutathione; TPL/NPs: TPL-loaded in HA-VE/PBAEss NPs; GPC: Gel permeation chromatography; DLE: Drug loading efficiency; DEE: drug entrapment efficiency; DLS: Dynamic light scattering; TEM: Transmission electron microscopy; FT-IR: Fourier transform infrared spectroscopy; XRD: X-ray diffraction; FCM: Fow cytometry; CLSM: Confocal laser scanning microscopy; H&E: Hematoxylin and eosin; E-cad: E-cadherin; ALT: Alanine aminotransferase; AST: Aspirate aminotransferase; BUN: Urea nitrogen; Cr: Creatinine.

Declarations

Author information

Jinfeng Shi and Yali Ren contributed equally to this study.

Affiliations

State Key Laboratory of Southwestern Chinese Medicine Resources, Pharmacy School, Chengdu University of Traditional Chinese Medicine, Chengdu, China

Jinfeng Shi†, Yali Ren†, Jiaqi Ma, Xi Luo, Jiaxin Li, Yihan Wu, Huan Gu, Chaomei Fu, Zhixing Cao*, Jinming Zhang*

Contributions

Jinfeng Shi: Investigation, Writing-original draft preparation, Writing-review and editing. **Yali Ren:** Conceptualization, Software, Writing-original draft preparation, Writing-review and editing. **Jiaqi Ma:** Validation, Investigation. **Xi Luo:** Validation, Investigation. **Jiaxin Li:** Methodology. **YihanWu:** Methodology. **HuanGu:** Methodology, Data curation. **ChaomeiFu:** Formal analysis. **ZhixingCao:** Conceptualization, Visualization. **Jinming Zhang:** Conceptualization, Resources, Writing-original draft preparation, Writing-review and editing, Supervision, Project administration, Funding acquisition. All data

were generated in-house, and no paper mill was used. All authors agree to be accountable for all aspects of work ensuring integrity and accuracy.

Corresponding author

Correspondence to Jinming Zhang or Zhixing Cao

Funding

This work was supported by Young Elite Scientists Sponsorship Program by CAST (2018QNRC1-01), National Natural Science Foundation of China (No. 81973662).

Ethics declarations

Ethics approval and consent to participate

Obtained the animal experiment ethics certification of Chengdu University of Traditional Chinese Medicine (CDUTCM, permit CDU2019S121).

Consent for publication

All the authors have approved the manuscript and agree to publication.

Availability of data and materials

All data generated or analyzed during this study are included in this published article [and its supplementary information files].

Competing Interest

The authors report no competing interests.

Supporting materials

Supplementary data associated with this article can be found in the online version.

References

1. Siegel RL, Miller KD, Jemal A. Cancer statistics, 2016. CA Cancer J Clin. 2016;66(1):7-30.
2. Sambi M, Qorri B, Harless W, Szewczuk MR. Therapeutic Options for Metastatic Breast Cancer. Adv Exp Med Biol. 2019;1152131-72.
3. Peart O. Metastatic Breast Cancer. Radiol Technol. 2017;88(5):519-39.
4. Hou W, Liu B, Xu HT. Triptolide: Medicinal chemistry, chemical biology and clinical progress. Eur J Med Chem. 2019;176378-92.

5. Noel P, Von Hoff DD, Saluja AK, Velagapudi M, Borazanci E, Han H. Triptolide and Its Derivatives as Cancer Therapies. Trends Pharmacol Sci. 2019;40(5):327-41.
6. Reno TA, Kim JY, Raz DJ. Triptolide Inhibits Lung Cancer Cell Migration, Invasion, and Metastasis. Ann Thorac Surg. 2015;100(5):1817-24.
7. Zheng W, Wang C, Ding RH, Huang YH, Li YY, Lu Y. Triptolide-loaded nanoparticles targeting breast cancer in vivo with reduced toxicity. Int J Pharm. 2019;572118721.
8. Xu H, Liu B. Triptolide-targeted delivery methods. Eur J Med Chem. 2019;164342-51.
9. Yuan ZX, Wu XJ, Mo J, Wang YL, Xu CQ, Lim LY. Renal targeted delivery of triptolide by conjugation to the fragment peptide of human serum albumin. Eur J Pharm Biopharm. 2015;94363-71.
10. He QL, Minn I, Wang Q, Xu P, Head SA, Datan E, Yu B, Pomper MG, Liu JO. Targeted Delivery and Sustained Antitumor Activity of Triptolide through Glucose Conjugation. Angew Chem Int Ed Engl. 2016;55(39):12035-9.
11. Nascimento TL, Hillaireau H, Vergnaud J, Fattal E. Lipid-based nanosystems for CD44 targeting in cancer treatment: recent significant advances, ongoing challenges and unmet needs. Nanomedicine (Lond). 2016;11(14):1865-87.
12. Luo Z, Dai Y, Gao H. Development and application of hyaluronic acid in tumor targeting drug delivery. Acta Pharm Sin B. 2019;9(6):1099-112.
13. Liu R, Hu C, Yang YY, Zhang JQ, Gao HL. Theranostic nanoparticles with tumor-specific enzyme-triggered size reduction and drug release to perform photothermal therapy for breast cancer treatment. Acta Pharm Sin B. 2019;9(2):410-20.
14. Zhang JM, Li JJ, Shi Z, Yang Y, Xie X, Lee SM, Wang YT, Leong KW, Chen MW. pH-sensitive polymeric nanoparticles for co-delivery of doxorubicin and curcumin to treat cancer via enhanced pro-apoptotic and anti-angiogenic activities. Acta Biomater. 2017;58349-64.
15. Chen FQ, Zhang JM, Wang L, Wang YT, Chen MW. Tumor pH(e)-triggered charge-reversal and redox-responsive nanoparticles for docetaxel delivery in hepatocellular carcinoma treatment. Nanoscale. 2015;7(38):15763-79.
16. Raza A, Hayat U, Rasheed T, Bilal M, Iqbal HMN. Redox-responsive nano-carriers as tumor-targeted drug delivery systems. Eur J Med Chem. 2018;157705-15.
17. Kong C, Li Y, Liu Z, Ye J, Wang Z, Zhang L, Kong W, Liu H, Liu C, Pang H, et al. Targeting the Oncogene KRAS Mutant Pancreatic Cancer by Synergistic Blocking of Lysosomal Acidification and Rapid Drug Release. ACS Nano. 2019;13(4):4049-63.
18. Wang Y, Liu X, Wang X, Zheng W, Zhang J, Shi F, Liu J. Redox-responsive self-assembly PEG nanoparticle enhanced triptolide for efficient antitumor treatment. Sci Rep. 2018;8(1):12968.
19. Luo ZJ, Dai Y, Gao HL. Development and application of hyaluronic acid in tumor targeting drug delivery. Acta Pharm Sin B. 2019;9(6):1099-112.
20. Vasi AM, Popa MI, Butnaru M, Dodi G, Verestiuc L. Chemical functionalization of hyaluronic acid for drug delivery applications. Mater Sci Eng C Mater Biol Appl. 2014;38177-85.

21. Abu-Fayyad A, Nazzal S. Gemcitabine-vitamin E conjugates: Synthesis, characterization, entrapment into nanoemulsions, and in-vitro deamination and antitumor activity. Int J Pharm. 2017;528(1-2):463-70.
22. Tan BJ, Chiu GN. Role of oxidative stress, endoplasmic reticulum stress and ERK activation in triptolide-induced apoptosis. Int J Oncol. 2013;42(5):1605-12.
23. Varghese E, Samuel SM. Triptolide Decreases Cell Proliferation and Induces Cell Death in Triple Negative MDA-MB-231 Breast Cancer Cells. Biomolecules. 2018;8(4): 7229-49.
24. Zhong L, Xu L, Liu YY, Li QS, Zhao DY, Li ZB, Zhang HC, Zhang HT, Kan QM, Wang YJ, et al. Transformative hyaluronic acid-based active targeting supramolecular nanoplatform improves long circulation and enhances cellular uptake in cancer therapy. Acta Pharm Sin B. 2019;9(2):397-409.
25. Yang XY, Cai XQ, Yu AH, Xi YW, Zhai GX. Redox-sensitive self-assembled nanoparticles based on alpha-tocopherol succinate-modified heparin for intracellular delivery of paclitaxel. J Colloid Interface Sci. 2017;496311-26.
26. Zhang HD, Jiang LH, Hou JC, Zhong SL, Zhou SY, Zhu LP, Li J, Wang DD, Sun DW, Ji ZL, Tang JH. Circular RNA hsa_circ_0052112 promotes cell migration and invasion by acting as sponge for miR-125a-5p in breast cancer. Biomed Pharmacother. 2018;1071342-53.
27. Padmanaban V, Krol I, Suhail Y, Szczerba BM, Aceto N, Bader JS, Ewald AJ. E-cadherin is required for metastasis in multiple models of breast cancer. Nature. 2019;573(7774):439-44.
28. Chen SR, Dai Y, Zhao J, Lin L, Wang Y, Wang Y. A Mechanistic Overview of Triptolide and Celastrol, Natural Products from Tripterygium wilfordii Hook F. Front Pharmacol. 2018;9104.
29. Chen H, Chen Q, Jiang CM, Shi GY, Sui BW, Zhang W, Yang LZ, Li ZY, Liu L, Su YM, et al. Triptolide suppresses paraquat induced idiopathic pulmonary fibrosis by inhibiting TGFB1-dependent epithelial mesenchymal transition. Toxicol Lett. 2018;2841-9.
30. Xie CM, Jiang J, Liu JP, Yuan GH, Zhao ZY. Triptolide suppresses human synoviocyte MH7A cells mobility and maintains redox balance by inhibiting autophagy. Biomed Pharmacother. 2019;115108911.
31. Zhao Y, Tan YN, Meng TT, Liu X, Zhu Y, Hong Y, Yang XQ, Yuan H, Huang X, Hu FQ. Simultaneous targeting therapy for lung metastasis and breast tumor by blocking the NF-κB signaling pathway using Celastrol-loaded micelles. Drug Deliv. 2018;25(1):341-52.
32. Song Y, Cai H, Yin TJ, Huo MR, Ma P, Zhou JP, Lai WF. Paclitaxel-loaded redox-sensitive nanoparticles based on hyaluronic acid-vitamin E succinate conjugates for improved lung cancer treatment. Int J Nanomedicine. 2018;131585-600.
33. Xu YQ, Liu DX, Hu J, Ding PR, Chen MW. Hyaluronic acid-coated pH sensitive poly (β-amino ester) nanoparticles for co-delivery of embelin and TRAIL plasmid for triple negative breast cancer treatment. Int J Pharm. 2020;573118637.
34. Wang W, Chen JR, Li M, Jia HZ, Han XX, Zhang JX, Zou Y, Tan BY, Liang W, Shang YY, et al. Rebuilding Postinfarcted Cardiac Functions by Injecting TIIA@PDA Nanoparticle-Cross-linked ROS-Sensitive Hydrogels. ACS Appl Mater Interfaces. 2019;11(3):2880-90.

35. Xu C, Song RJ, Lu P, Chen JC, Zhou YQ, Shen G, Jiang MJ, Zhang W. pH-triggered charge-reversal and redox-sensitive drug-release polymer micelles codeliver doxorubicin and triptolide for prostate tumor therapy. Int J Nanomedicine. 2018;137229-49.
36. Liu XR, Wang C, Ma HS, Yu FY, Hu FQ, Yuan H. Water-Responsive Hybrid Nanoparticles Codelivering ICG and DOX Effectively Treat Breast Cancer via Hyperthermia-aided DOX Functionality and Drug Penetration. Adv Healthc Mater. 2019;8(8):e1801486.

Figures

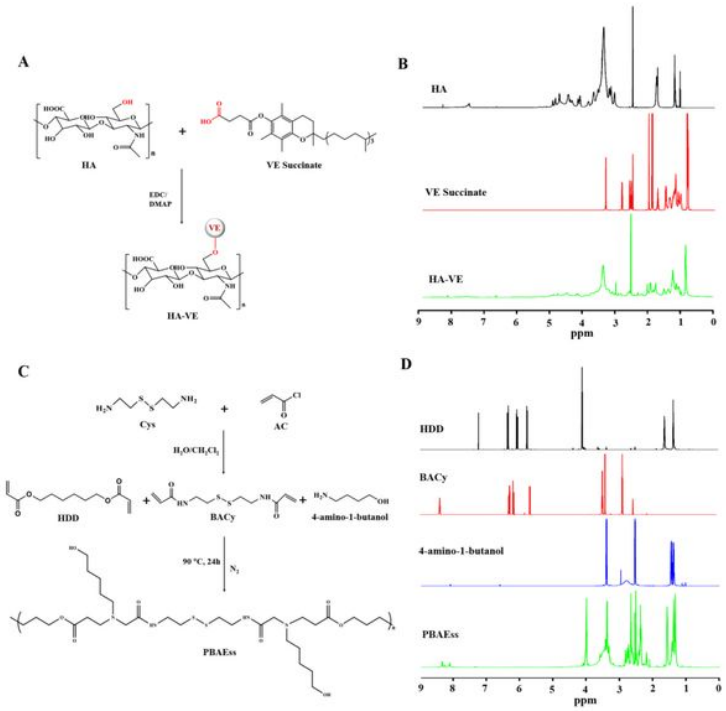

Figure 1

(A) Synthesis route of HA-VE conjugate. (B) 1H NMR spectra of HA, VE and HA-VE in DMSO-d6. (C) Synthesis route of PBAEss copolymer. (D) 1H NMR spectra of HDD, BACy, 4-amino-1-butanol and PBAEss in CDCl3.

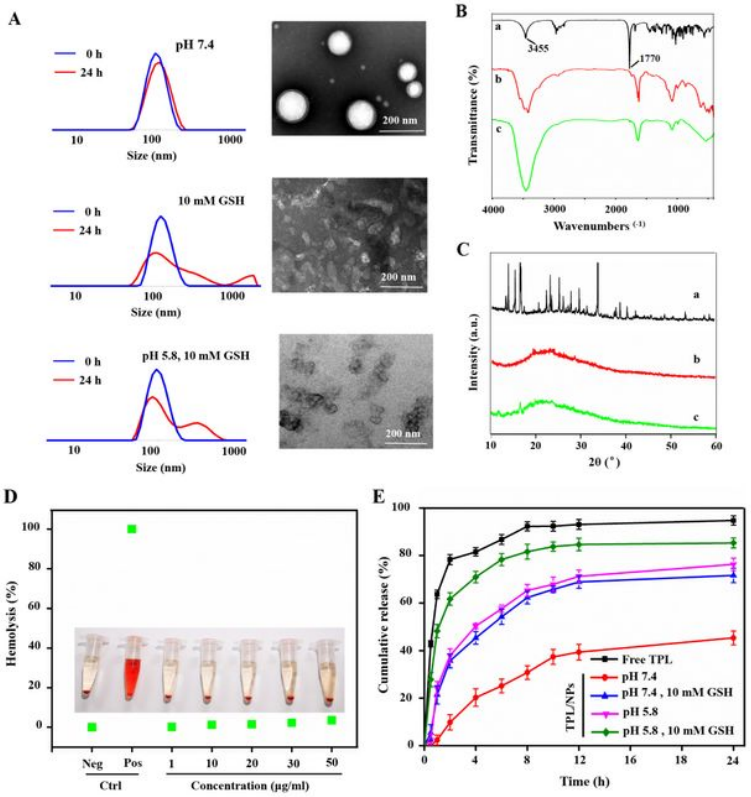

Figure 2

Characterization of TPL/NPs. (A) Particle distribution by DLS and TEM image of TPL/NPs in response to different conditions. FT-IR (B) and XRD (C) analysis of TPL/NPs. (a: Free TPL; b: TPL + polymer; c: TPL/NPs). (D) Hemolysis assay of TPL/NPs at different concentrations of HA-VE/PBAEss polymers. PBS and water were employed as negative and positive control, responsively. (E) In vitro release profile of TPL from TPL/NPs in different medium at 37˚C.

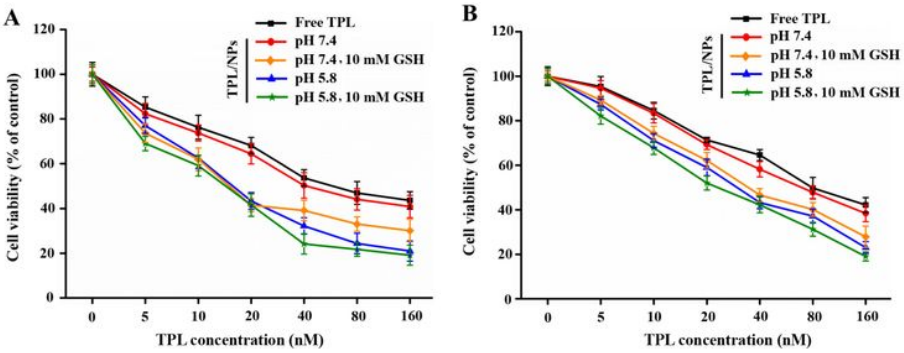

C

Groups		IC50 (nM)	
		MCF-7	MDA-MB-231
Free TPL		77.38 ± 5.6	88.71 ± 4.3
TPL/NPs	pH 7.4	58.67 ± 2.7	72.28 ± 5.6
	pH 7.4、10 mM GSH	20.76 ± 6.2	41.77 ± 5.1
	pH 5.8	18.11± 3.2	34.14 ± 4.7
	pH 5.8、10 mM GSH	13.77 ± 3.4	26.39 ± 3.3

Figure 3

Cytotoxicity of TPL/NPs against MDA-MB-231 (A) and MCF-7 (B) cells for 48 h treatment in different culture media. (C) IC50 values of TPL/NPs in MDA-MB-231 and MCF-7 cells with 48 h treatment were calculated and listed.

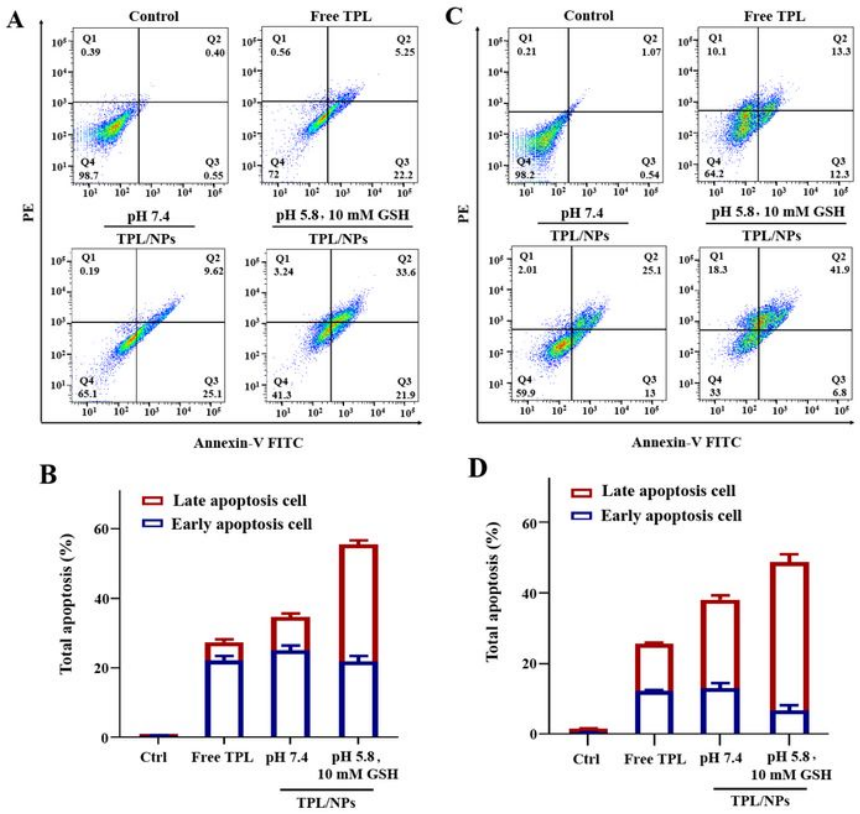

Figure 4

Representative images of Annexin V-FITC and PI staining of MDA-MB-231 (A) and MCF-7 (C) cells treated with TPL/NPs (20 nM) for 24 h. Quantification results of TPL/NPs on apoptosis induction of MDA-MB-231 (B) and MCF-7 (D) cells.

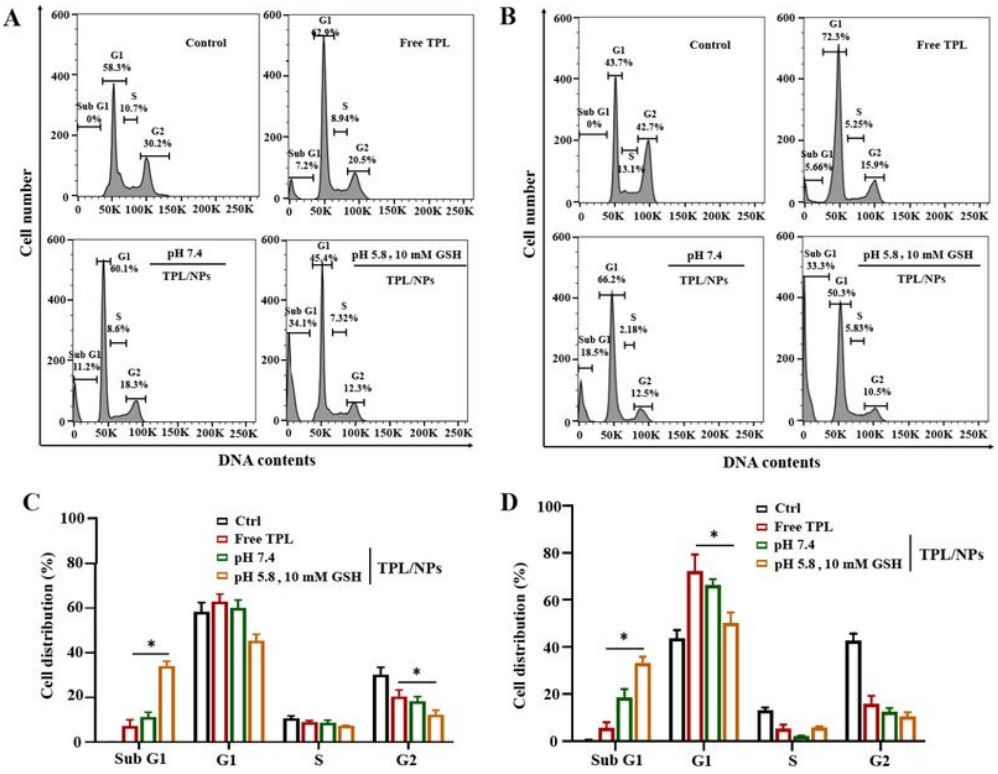

Figure 5

Representative cell cycle distribution histograms of MDA-MB-231 (A) and MCF-7 (B) cells treated by TPL/NPs for 24 h. Relative cell cycle distribution of Sub G1, G1, S and G2 phase for MDA-MB-231 (C) and MCF-7 (D) cells.

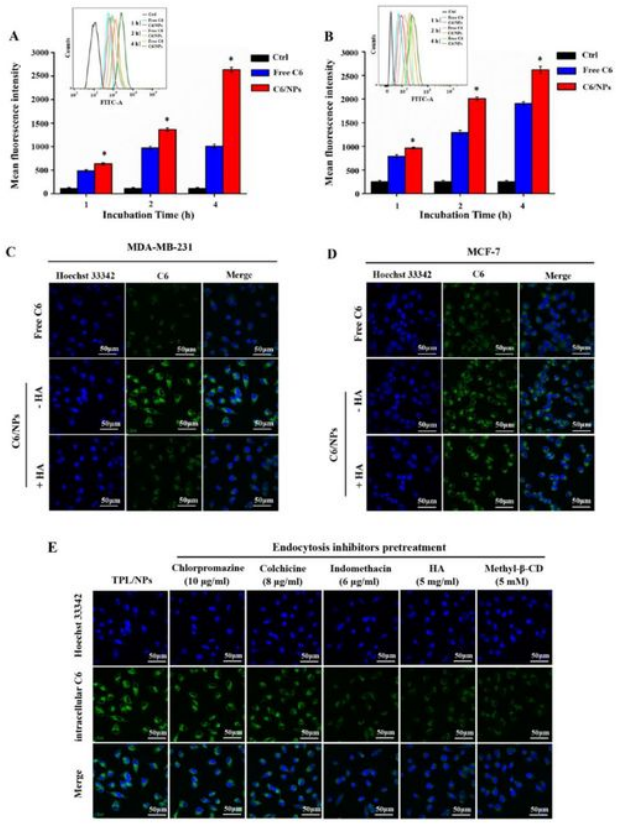

Figure 6

Intracellular fluorescence of MDA-MB-231 (A) and MCF-7 (B) cells determined by FCM, which were treated by either free C6 or C6/NPs for 1h, 2h and 4h, respectively. The representative cellular uptake images of MDA-MB-231 (C) and MCF-7 (D) cells after incubated with free C6 and C6/NPs for 4 h by CLSM observation. The cellular uptake images of C6/NPs in MDA-MB-231 cells with some endocytosis inhibitors pretreated (E). Note: *P<0.05 C6/NPs versus free C6 group.

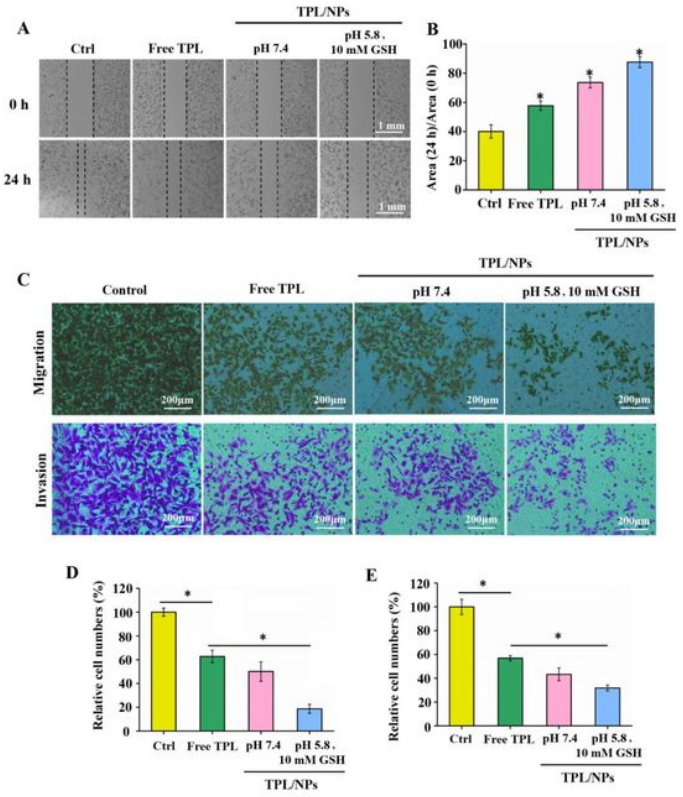

Figure 7

Effects of TPL/NPs on MDA-MB-231 cell migration and invasion. (A) Images of wound healing assays (magnification, ×100). Cells seeded into 12-well cell culture plates and cultured to near confluency. The wounded monolayer was treated with PBS, free TPL, TPL/NPs at media pH 7.4 and TPL/NPs at the medium of pH 5.8, 10 mM GSH for 24 h. (B) Scratch area measured with ImageJ software. (C) Photographs of migration and invasion MDA-MB-231 cells with different treatments using the Transwell chamber. Percent of cell migration (D) and invasion (E).

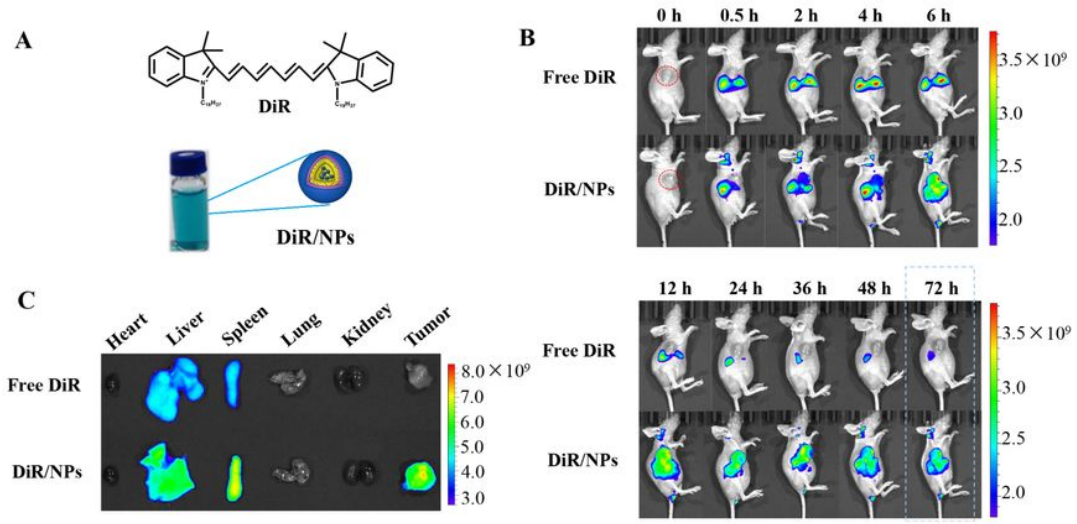

Figure 8

Tumor targeting profiles of HA-VE/PBAEss NPs in vivo by IVIS spectrum. (A) The schematic diagram to prepare the fluorescent NPs using DiR dye loaded in HA-VE/PBAEss NPs with the similar approach as TPL/NPs. (B) Fluorescent distribution of DiR/NPs in vivo after vein injection at predetermined time intervals, i.e., 0, 0.5, 2, 4, 6, 12, 24, 36, 48 and 72 h after injection. (C) Ex vivo fluorescence images of dissected organs of the mice for 72 h post-injection.

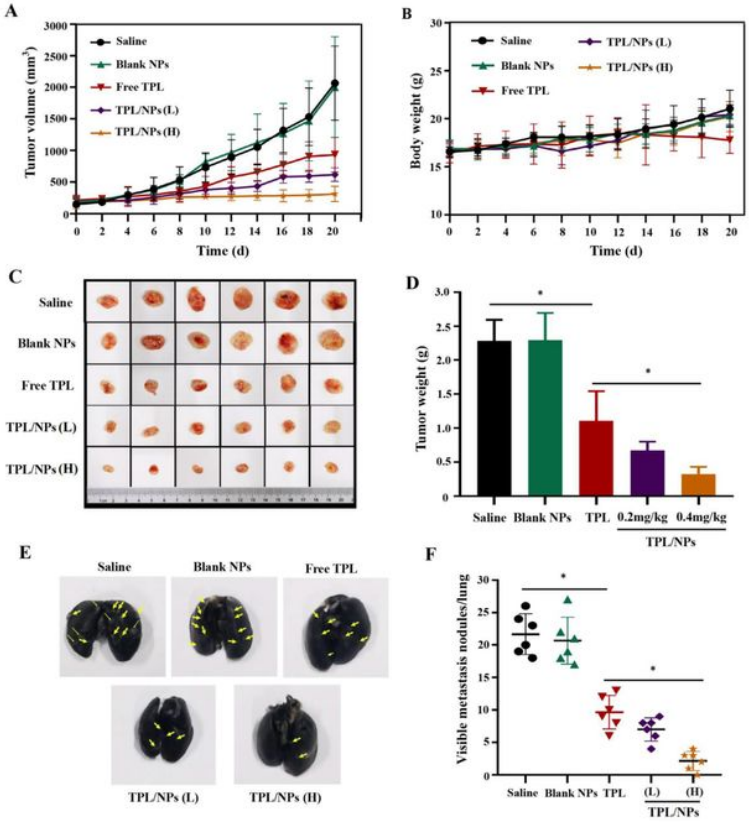

Figure 9

In vivo the suppression activities of TPL/NPs to primary tumor and lung metastasis on 4T1 xenograft model. (A) Growth curve of the 4T1 xenografts in BALB/c mice treated with saline, blank NPs, free TPL, TPL/NPs (L), and TPL/NPs (H)) for 20 days. Data were presented as the mean ± standard error (SD, n = 6 mice). (B) Body weight as a function of time. (C) Picture of excised tumors at the end of the experiment. (D) Tumor weight at the end of the experiment. (E) Representative photograph of the 4T1 mouse lungs with the Indiaink stained whole lungs at the end of the experiment. Representative tumors are marked by arrows. (F) Semiquantitative analysis of metastatic nodules in lungs at the end of the experiment when treated with saline, blank NPs, free TPL, TPL/NPs (L), and TPL/NPs (H)) for 20 days. Note: *p<0.05.

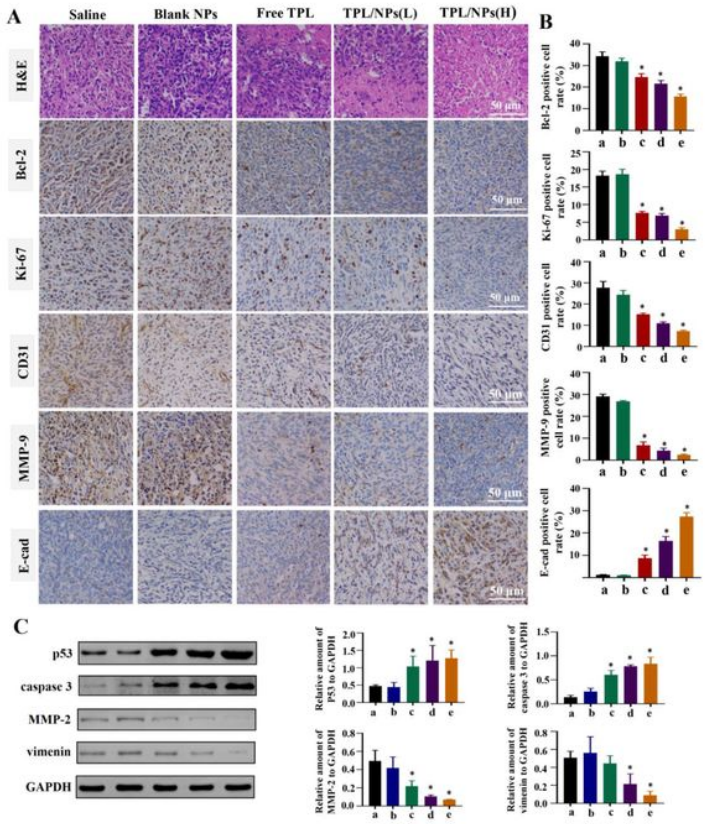

Figure 10

Histological staining and western blot analysis of representative proteins in tumor sections derived from mice treated with saline, free TPL, Blank NPs, TPL/NPs(L) and TPL/NPs(H), respectively. (A) H&E staining and immunohistochemistry staining of Bcl-2, Ki-67, CD31, MMP-9 and E-cad; (B) Statistical analysis for the percentage of Bcl-2, Ki-67, CD31, MMP-9 and E-cad expression in the tumor sections by immunohistochemistry staining. The expression of EMT-relative proteins (MMP-2 and vimentin) and mitochondrial apoptosis pathway-relative proteins (p53 and caspase 3) were evaluated by Western blot (C). Semi-quantification of the expression level of these proteins (D). Note: *p<0.05.

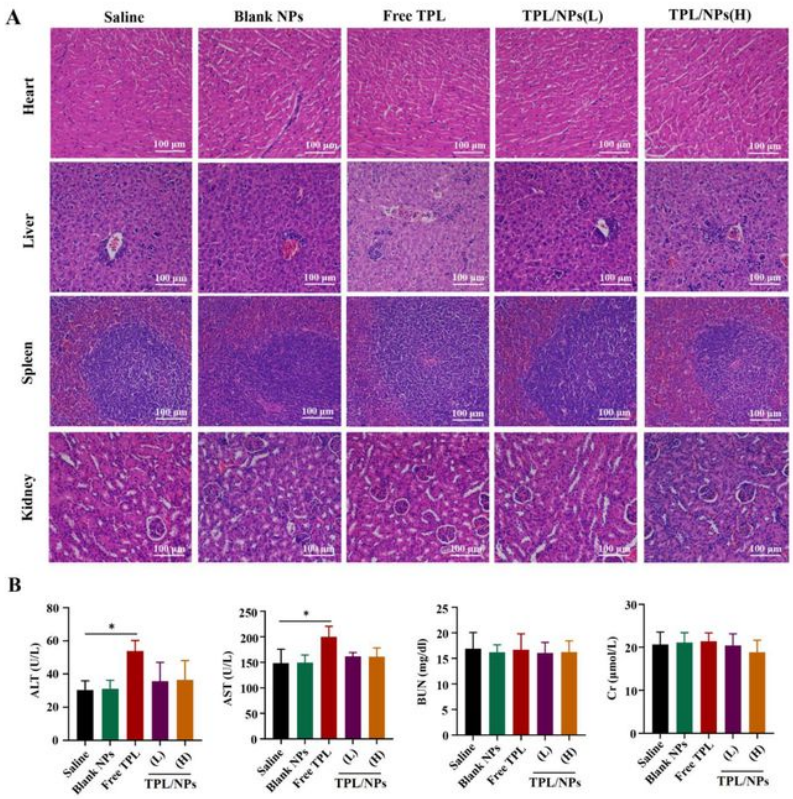

Figure 11

The systemic toxicity in tumor bearing mice treated with saline, free TPL, Blank NPs, TPL/NPs(L) and TPL/NPs(H), respectively. (A) Histopathological changes in heart, liver, spleen and kidney tissues. (B) ALT, AST, BUN and Cr levels in serum of the mice at the therapeutic end point of different treatments. Note: *p<0.05.

Supplementary Files

This is a list of supplementary files associated with this preprint. Click to download.

- Supplementarymaterials.docx